NMDA receptor surface mobility depends on NR2A-2B subunits

Laurent Groc, Martin Heine, Sarah L. Cousins, F. Anne Stephenson, Brahim Lounis, Laurent Cognet, and Daniel Choquet

PNAS published online Nov 21, 2006;
doi:10.1073/pnas.0605238103

NMDA receptor surface mobility depends on NR2A-2B subunits

Laurent Groc*†, Martin Heine*, Sarah L. Cousins‡, F. Anne Stephenson‡, Brahim Lounis§, Laurent Cognet§, and Daniel Choquet*

*Physiologie Cellulaire de la Synapse, Unité Mixte de Recherche (UMR) 5091, Centre National de la Recherche Scientifique (CNRS), Université Bordeaux 2, 33077 Bordeaux, France; §Centre de Physique Moléculaire Optique et Hertzienne, CNRS-UMR 5798, Université Bordeaux 1, 33405 Talence, France; and ‡School of Pharmacy, University of London, 29/39 Brunswick Square, London WC1N 1AX, United Kingdom

Edited by Richard L. Huganir, Johns Hopkins University School of Medicine, Baltimore, MD, and approved September 29, 2006 (received for review June 22, 2006)

The NR2 subunit composition of NMDA receptors (NMDARs) varies during development, and this change is important in NMDAR-dependent signaling. In particular, synaptic NMDAR switch from containing mostly NR2B subunit to a mixture of NR2B and NR2A subunits. The pathways by which neurons differentially traffic NR2A- and NR2B-containing NMDARs are poorly understood. Using single-particle and -molecule approaches and specific antibodies directed against NR2A and NR2B extracellular epitopes, we investigated the surface mobility of native NR2A and NR2B subunits at the surface of cultured neurons. The surface mobility of NMDARs depends on the NR2 subunit subtype, with NR2A-containing NMDARs being more stable than NR2B-containing ones, and NR2A subunit overexpression stabilizes surface NR2B-containing NMDARs. The developmental change in the synaptic surface content of NR2A and NR2B subunits was correlated with a developmental change in the time spent by the subunits within synapses. This suggests that the switch in synaptic NMDAR subtypes depends on the regulation of the receptor surface trafficking.

development | glutamate receptor | lateral mobility

NMDA receptors (NMDARs) are heterotetrameric cation channels composed of NR1 and NR2/3 subunits (1). NMDARs are assembled early in the endoplasmic reticulum, and both NR1 and NR2 subunits are necessary for their association and their successful cell surface targeting (2). In addition to glutamate and glycine, NMDARs require membrane depolarization to open with high probability (3), making this receptor a pre- and postsynaptic activity coincident detector involved in the induction of Hebbian synaptic plasticity. The functional properties of NMDARs depend also on the subunit composition, and such subunit heterogeneity of synaptic NMDARs is thought to play an important role during synaptic development, maturation, and plasticity processes (4). During synaptic development, the subunit composition of synaptic NMDARs changes from heterodimers containing predominantly NR2B subunits at early stages to heterodimers containing NR1/NR2B, NR1/NR2A, and NR1/NR2A/NR2B subunits at mature stage (1, 5–14). This change often is associated with the refinement of neuronal connections within cortical areas, although this model has been challenged and, thus, is likely incomplete (4). The pathways by which neurons differentially traffic NR2A- and NR2B-containing NMDARs remain, however, an open question of crucial importance to understand the shaping of synaptic maturation and plasticity.

Changes in NR2 subunit composition of NMDARs within synapses can be triggered by mechanisms that include differences in insertion (15), internalization (16, 17), and/or lateral diffusion. Interestingly, NMDARs diffuse laterally at the neuronal surface (18, 19). In immature neurons, synaptic NMDARs are replaced rapidly by extrasynaptic ones through lateral diffusion (18), suggesting that surface mobility of NMDARs may be involved in shaping mature NMDAR synaptic components. In this study, we investigated the surface mobility of NR2A- and NR2B-containing NMDARs by using single-particle and single-molecule approaches. To selectively discriminate between these NMDAR types, we used antibodies directed against specific extracellular epitopes of these two subunits. Our results indicate that the surface mobility of NR2A-containing NMDARs is much smaller than that of NR2B-containing ones. During neuronal maturation, the decreased contribution of synaptic surface NR2B-containing NMDARs correlated with decreases in synaptic stabilization of the more mobile NR2B-containing NMDARs.

Results

Specific Detection of NR2A and NR2B Subunits. To selectively track surface NR2A- and NR2B-containing NMDARs, polyclonal antibodies directed against extracellular epitopes of NR2A subunit was developed, and a previously described antibody directed against NR2B subunit were used (20, 21). As shown in Fig. 1*a*, the peptide sequences used for antibody production correspond to amino acid sequences in the N-terminal domain of the NR2 subunits. Importantly, an alignment of the two peptide sequences, peptide NR2A versus full-length NR2B and peptide NR2B versus full-length NR2A, show no amino acid sequence similarity. To test the specificity of the NR2A antibody, HEK293 cells were transfected with NR1/NR2A, NR1/NR2B, NR1/NR2C, or NR1/NR2D subunit cDNAs, total cell homogenates were prepared and analyzed by immunoblotting with either anti-NR2A (44–58) antibodies (Fig. 1*b*), anti-NR2A antibodies (1454–1464) (Fig. 1*c*) that recognize both NR2A and NR2B subunits, or anti-NR2D antibodies (1307–1323) (Fig. 1*c*) that recognize both NR2C and NR2D subunits (22). As shown in Fig. 1*b*, the anti-NR2A (44–58) antibody recognizes only recombinant NR2A subunits. To further test the antibody specificity, P2 fractions prepared from whole brain of either wild-type or NR2A (−/−) mice were analyzed by immunoblotting with anti-NR2A (44–58) or anti-NR2A (1454–1464) antibodies (Fig. 1*d*). As predicted, anti-NR2A (44–58) antibodies did not recognize a M_r 180-kDa immunoreactive species in the P2 fractions prepared from NR2A (−/−) mice (Fig. 1*d*). In an additional control, HEK293 cells were transfected with either NR1/NR2A or NR1/NR2B subunit cDNAs, and cell surface ELISAs were carried out, as described in ref. 21 by using either anti-NR2A (44–58) or anti-NR2B (42–60) antibodies (Fig. 1 *e* and *f*). It can be seen that anti-NR2A (44–58) antibodies recognize mostly cell surface-expressed NR2A subunits and anti-NR2B (42–60), NR2B subunits only (Fig. 1*e*). For total staining, the cells first were permeabilized

Author contributions: L.G. and D.C. designed research; L.G. and M.H. performed research; S.L.C., F.A.S., B.L., and L.C. contributed new reagents/analytic tools; L.G. analyzed data; and L.G. wrote the paper.

The authors declare no conflict of interest.

This article is a PNAS direct submission.

Abbreviations: IQR, interquartile range; NMDAR, NMDA receptor; QD, quantum dot.

†To whom correspondence should be addressed. E-mail: laurent.groc@u-bordeaux2.fr.

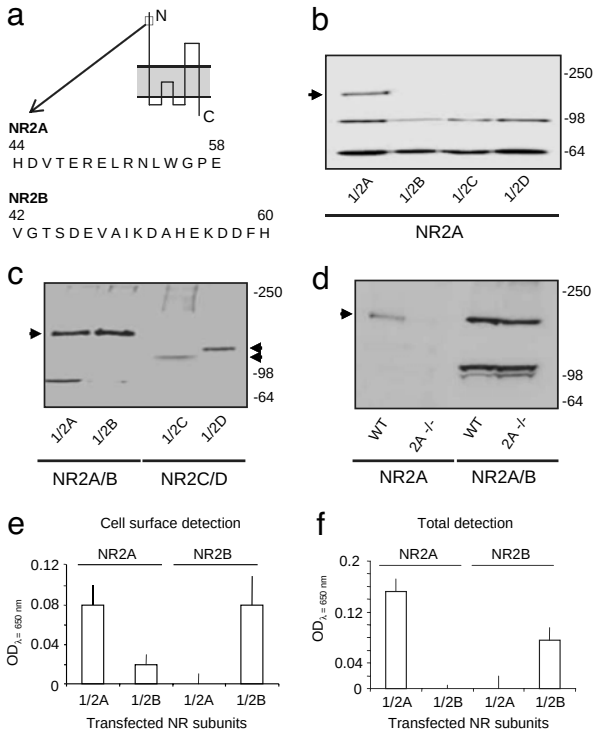

Fig. 1. Characterization of anti-NR2A and anti-NR2B antibodies. (*a*) Peptide sequences from the N-terminal domain of NR2A (44–58) and NR2B (42–60) subunits used to raise antibodies. (*b*) HEK293 cells were transfected with either NR1/NR2A, NR1/NR2B, NR1/NR2C, or NR1/NR2D subunit cDNAs. Cells were analyzed by immunoblotting with an anti-NR2A (44–58) antibody. Note the specific detection of NR2A subunit (arrow). (*c*) Using the same method as in *b*, NR2A, NR2B, NR2C, or NR2D subunit was detected by using either an anti-NR2A antibody (1454–1464) that recognizes both NR2A (M_r 180 kDa) and NR2B (M_r 180 kDa) subunits (left arrowhead in lanes 1 and 2) or an anti-NR2D antibody (1307–1323) that recognizes both NR2C (M_r 135 kDa, right lower arrowhead) and NR2D (150 kDa, right upper arrowhead) (lanes 3 and 4). The positions of molecular mass standards (kDa) are shown on the right. (*d*) P2 fractions were prepared from whole brain (15 μg of wet weight tissue applied per gel lane) of either wild-type (WT) or NR2A ($-/-$) mice and analyzed by immunoblotting with anti-NR2A (44–58) or anti-NR2A (1454–1464) antibodies. In lane 2, note that the anti-NR2A (44–58) antibody does not recognize an immunoreactive species in the P2 fractions prepared from NR2A ($-/-$) mice. (*e* and *f*) HEK293 cells were transfected with either NR1/NR2A or NR1/NR2B NMDA receptor subunit cDNAs and cell surface ELISAs carried out by using either anti-NR2A (44–58) or anti-NR2B (42–60) antibodies as indicated. It can be seen that anti-NR2A (44–58) antibodies recognize only cell surface-expressed NR2A subunits and anti-NR2B (42–60), NR2B subunits only (means ± SD for triplicate values, $n = 3$).

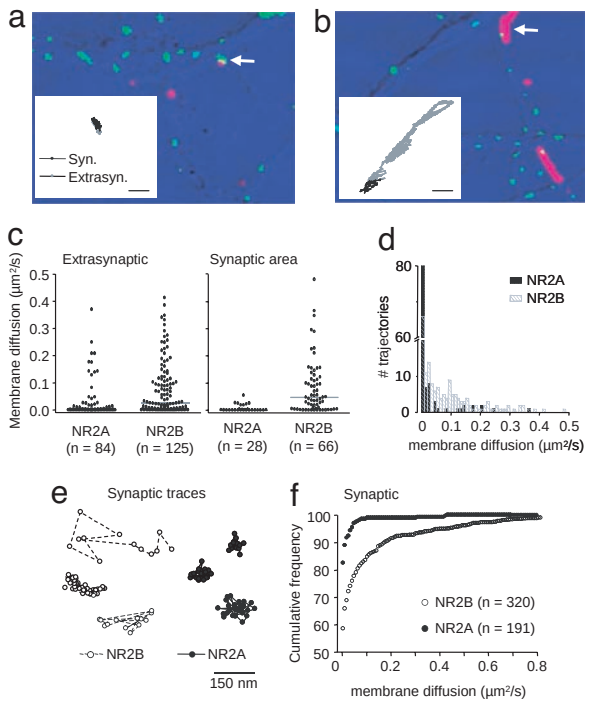

Fig. 2. Differential membrane diffusion of NR2A- and NR2B-containing NMDARs at the surface of D15 neurons. (*a* and *b*) Representative summed trajectories of QD coupled to NR2A- (*a*) and NR2B-containing (*b*) NMDARs. The green spots represent synaptic sites labeled with Mitotracker. The red traces represent the trajectory of QD–NR2 subunit complexes, with immobile complexes being exemplified by dot-like trajectory, whereas diffusing complexes are represented by extended line trajectories. (*c*) Scatter plot distributions of the instantaneous diffusion coefficient of NR2A- and NR2B-containing NMDARs in the extrasynaptic (*Left*) and the synaptic area (*Right*). The bar in each group represents the median value. (*d*) Superimposed distribution histograms of the instantaneous diffusion coefficient of NR2A- (filled bars) and NR2B- (hatched gray bars) containing NMDARs. Note the overlap for the low diffusion coefficients. (*e*) Examples of NR2A- (filled dots, full line) and NR2B-containing NMDAR (open dots, broken line) trajectories obtained by single-molecule approach within synapses (Scale bar: 150 nm.) (*f*) Cumulative distributions of the instantaneous diffusion coefficient of synaptic NR2A- (filled dots) and NR2B-containing (open dots) NMDARs. The first point of the distributions corresponds to the percentage of immobile receptors (bin size = 0.0075 $\mu m^2/s$). Note the higher percentage of immobile synaptic NR2A- (83%) when compared with NR2B-containing (59%) NMDARs.

with 0.25% Triton X-100, and then antibody was added for incubation. The same conclusion regarding antibody specificity was reached (Fig. 1*f*). Finally, we tested the specificity of antibodies by labeling live HEK cells double-transfected with the NR1 coupled to yellow fluorescent protein and either NR2A or NR2B subunit cDNAs. The presence of membrane NR2A subunits then was revealed by using the anti-NR2A (44–58) antibodies. We found that only NR1-positive HEK cells that were cotransfected with NR2A subunit cDNAs displayed NR2A subunit surface staining, whereas cells cotransfected with NR2B subunit cDNAs displayed no NR2A subunit surface staining (data not shown). All together, the data indicate that these newly generated anti-NR2A and anti-NR2B antibodies can be used in live cells to discriminate between surface-exposed NR2A or NR2B subunit, respectively.

Differential Surface Diffusion of NR2A- and NR2B-Containing NMDARs. Because NR2A- and NR2B-containing NMDARs have different surface distributions, we then measured and compared the surface mobility of both NR2A- and NR2B-containing NMDARs by using two approaches: (*i*) single-particle tracking based on the detection of quantum dots (QDs) and (*ii*) single-molecule tracking based on the detection of the single organic fluorophores, i.e., cyanine 3. QD-based tracking provides a unique tool for long-term recording of receptor surface diffusion because QDs are more photostable than organic dyes (19, 23). However, as reported in ref. 19, QD-based tracking may be biased to some extent within a confined space, so we also used the single-molecule approach to track synaptic receptors. To differentiate synaptic versus extrasynaptic receptors, synapses were labeled with the active mitochondria marker, Mitotracker (rhodamine derivative), which was shown to colocalize with the presynaptic synaptotagmin clusters (19, 24).

Representative summed trajectories recorded at days *in vitro* 15 and over a 60-s period time (reconstruction from image series acquired at 30 Hz rate), are shown in Fig. 3 *a* and *b*. The NR2A-containing NMDAR summed trajectories (a single red trace corresponds to the whole trajectory of a single QD–NR2A antibody complex) show that subunits are immobile or very slowly mobile in both synaptic (green spots) and extrasynaptic compartments (Fig. 2*a*). In contrast, the NR2B-containing NMDAR summed trajec-

tories show more heterogenous behaviors because highly mobile (red line) and immobile (red spot) trajectories are observed (Fig. 2*b*). In these examples, the mobile NR2B-containing NMDARs diffuse laterally in an area of several micrometers. Reconstructed trajectories for NR2A- (Fig. 2*a*) and NR2B-containing NMDARs (Fig. 2*b*) are shown in the insets. From the trajectories of each molecule, the instantaneous diffusion coefficient of extrasynaptic NR2A- and NR2B-containing NMDARs then were calculated. It was significantly lower for extrasynaptic NR2A-containing NMDAR than for extrasynaptic NR2B-containing ones (NR2A median = 7.5×10^{-4} $\mu m^2/s$, interquartile range (IQR) = 1.1×10^{-4}-0.013 $\mu m^2/s$, $n = 84$; NR2B median = 250×10^{-4} $\mu m^2/s$, IQR = 24×10^{-4}-0.115 $\mu m^2/s$, $n = 125$; $P < 0.001$, Mann–Whitney *U* test) (Fig. 2*c Left*). This difference can be accounted for variations in the percentage of immobile receptors and/or the diffusion of the mobile ones. To differentiate between these possibilities, we compared these parameters. The percentage of immobile extrasynaptic receptors was higher for the population of extrasynaptic NR2A-containing NMDARs (69%) when compared with the NR2B-containing ones (34%), whereas there was no significant difference in the diffusion of the respective mobile fraction (NR2A median = 0.04 $\mu m^2/s$, IQR = 0.01–0.16 $\mu m^2/s$, $n = 28$; NR2B median = 0.08 $\mu m^2/s$, IQR = 0.02–0.18 $\mu m^2/s$, $n = 82$; $P > 0.05$, Mann–Whitney *U* test). Thus, within the plasma membrane, extrasynaptic NR2A-containing NMDARs diffuse less than extrasynaptic NR2B-containing NMDARs because of a higher proportion of immobile receptors. Within the synaptic area (synapse plus 300-nm annulus), the same difference was observed: the NR2A-containing NMDARs diffused significantly less than NR2B-containing ones (NR2A median = 2×10^{-4} $\mu m^2/s$, IQR = 0–0.01 $\mu m^2/s$, $n = 28$; NR2B median = 500×10^{-4} $\mu m^2/s$, IQR = 43×10^{-4}-0.125 $\mu m^2/s$, $n = 665$; $P < 0.001$) (Fig. 2*c Right*) and the proportion of immobile NR2A-containing NMDARs was 2.5-fold higher than that of NR2B-containing NMDARs (75% versus 29%). We further compared subunit surface diffusion in the synapse by using the single-molecule approach. The instantaneous diffusion coefficient of NR2A-containing NMDAR diffusion was lower than that of NR2B-containing NMDARs. The percentage of immobile NR2A- and NR2B-containing NMDARs was 82% and 56%, respectively (Fig. 2 *e* and *f*). Thus, consistent with the QD-based data, the synaptic diffusions of surface NR2A- and NR2B-containing NMDARs are different.

Although our approach does not permit to target specifically NMDAR triheteromers (e.g., NR1/NR2A/NR2B), the current data indicate that NR2A-containing NMDAR membrane diffusion overlap the one of NR2B-containing NMDARs only for low-diffusion coefficients (Fig. 2*d*), implying that such triheteromers would diffuse within the plasma membrane with instantaneous coefficient <0.025 $\mu m^2/s$. To investigate whether NMDAR triheteromers have distinct properties, i.e., whether NR2A subunit expression affect the behavior of NR2B-containing NMDARs, we performed experiments in which the surface diffusion of NR2B-containing NMDARs were measured in neurons overexpressing either NR2B (*t*-NR2B) or NR2A (*t*-NR2A) subunits (Fig. 3 *a* and *b*; *Supporting Methods*, which is published as supporting information on the PNAS web site). Interestingly, the overexpression of NR2A subunits significantly reduced the surface diffusion of NR2B-containing NMDARs (*t*-NR2B median = 9×10^{-5} $\mu m^2/s$, IQR = 3.10^{-6} to 8.10^{-2} $\mu m^2/s$, $n = 927$; *t*-NR2A median = 5×10^{-6} $\mu m^2/s$, IQR = 0–9 $\times 10^{-4}$ $\mu m^2/s$, $n = 1{,}157$; $P < 0.001$, Mann–Whitney *U* test) (Fig. 3 *b* and *c*), by decreasing both the number of mobile receptors (*t*-NR2B = 32%; *t*-NR2A = 14%) and the membrane diffusion of the mobile ones (Fig. 3*d*). These results indicate that the presence of surface NR2A subunit influence the surface diffusion of NR2B-containing NMDARs, suggesting that NR2A subunit is present in NMDAR triheteromers and that NR2A subunit presence has a major role in NMDAR surface diffusion properties.

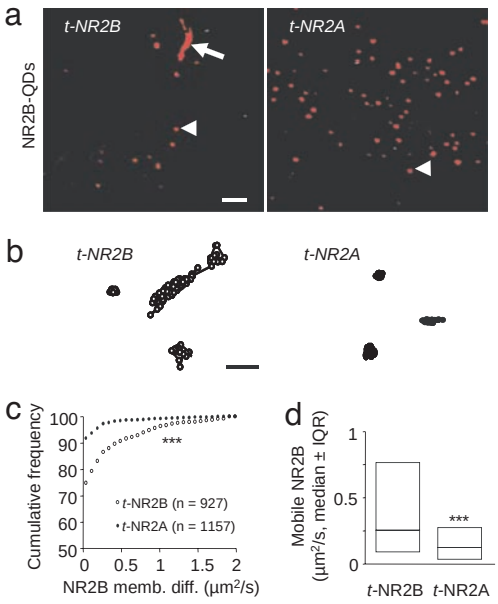

Fig. 3. Overexpression of NR2A subunit affect the surface diffusion of NR2B-containing NMDARs in days *in vitro* 10–15 hippocampal-cultured neurons. (*a*) Representative summed trajectories of QDs coupled to NR2B-containing NMDAR (red traces) recorded at the surface of transfected neurons by SEP-NR2B (*Left*) or SEP-NR2A (*Right*). QDs were only tracked at the somatic surface of SEP-NR-positive neurons to ensure that only NR2-overexpressing neurons were analyzed. Typical immobile trajectory of NR2B-containing NMDAR are indicated by arrowheads, whereas a diffusing NR2B-containing NMDAR is pointed out by an arrow line. (Scale bar: 1 μm.) (*b*) Examples of NR2B-containing NMDAR from SEP-NR2B-positive (*Left*, open circle) or SEP-NR2A-positive (Right, filled circle) neurons. (Scale bar: 175 nm.) (*c*) Cumulative distributions of the instantaneous diffusion coefficient of surface NR2B-containing NMDARs from neurons overexpressing either NR2B (NR2B *t*, open circle) or NR2A (NR2A *t*, filled circle) subunits (bin size = 0.075 $\mu m^2/s$). The NR2B-containing NMDAR surface diffusion was reduced significantly in neurons overexpressing NR2A subunits (***, $P < 0.001$, Mann–Whitney test). (*d*) The surface diffusion of mobile NR2B-containing NMDARs was significantly slower in NR2A-overexpressing neurons when compared with NR2B overexpressing ones (***, $P < 0.001$, Mann–Whitney test).

Native NR2A and NR2B Subunit Surface Diffusions and Distributions Overdevelopment. To investigate the developmental changes of NR2A and NR2B-containing NMDAR surface diffusion, we first performed live immunostainings of native NR2A- or NR2B-containing NMDARs at the surface of dendritic arbors (somatic staining was not considered) of live hippocampal cultured neurons at two different developmental stages: D7–9, referred as "D8" and D14–16, referred as "D15." In agreement with previous reports, surface NR2A and NR2B subunit immunostainings were different: (*i*) the dendritic surface NR2A subunit staining significantly increased during this period, whereas the surface density of NR2B subunit slightly, but not significantly, decreased during this period, and (*ii*) the percentage of NR2A subunit staining that colocalize with the presynaptic marker, synaptotagmin, significantly increased during this period, whereas the opposite trend was observed for NR2B subunit staining (Fig. 6, which is published as supporting information on the PNAS web site). Moreover, respective to function, we recorded NMDAR-mediated miniature excitatory postsynaptic currents (mEPSCs) at these two developmental stages (*Supporting Methods*). The NMDAR mEPSC decay time decreased from D8 to D15 neurons (D8 : two exponential fit: $\sigma_1 = 20 \pm 4$ ms and $\sigma_2 = 196 \pm 38$ ms, $n = 5$; D15 : $\sigma_1 = 9 \pm 4$ ms and $\sigma_2 = 91 \pm 17$ ms, $n = 5$), suggesting a functional switch in the NR2 subunit composition of synaptic NMDAR from NR2B-containing receptors to NR2A-containing ones, as previously reported by numerous studies with cultured neurons (5, 9, 12, 14, 25–27).

NEUROSCIENCE

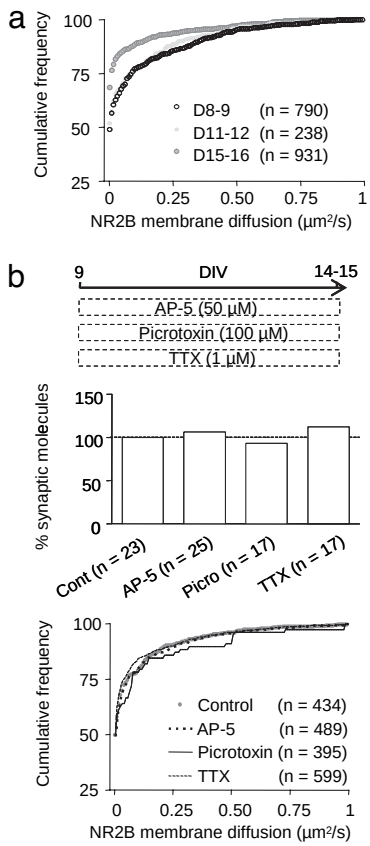

Fig. 4. The surface diffusion of NR2B-containing NMDARs decreases overdevelopment in an activity-independent manner. (*a*) Cumulative distributions of the instantaneous diffusion coefficient of extrasynaptic NR2B-containing NMDAR at three developmental stages: days *in vitro* (D)8–9 (open dots), D11–12 (gray dots), and D15–16 (dark gray dots) neurons. The first point of the distributions corresponds to the percentage of immobile receptors (bin size = 0.0075 $\mu m^2/s$). Note the significant diffusion decreases at D15–16 when compared with D8–9 ($P < 0.001$, Kolmogorov–Smirnov test). (*b*) Chronic treatments with AP5, tetrodotoxin (TTX), or picrotoxin were applied from D9 to D15 (*Top*) to block the global neuronal activity. None of these treatments affected the surface distribution of NR2B-containing NMDARs, as shown by the percent of synaptic molecules in all conditions ($P > 0.05$, n = number of dendritic fields examined) (*Middle*). The membrane diffusion distributions in all conditions were statistically not different (*Bottom*).

Based on these findings, we then asked whether such developmental change correlated with changes in surface diffusion of NR2B-containing NMDAR between D8 and D15. The diffusion of NR2B-containing NMDARs decreases significantly from D8 to D15, mostly because of a higher proportion of immobile receptors (first point in the cumulative curves) (Fig. 4*a*). We further tested whether surface diffusion and distribution of NR2B-containing NMDARs are modulated by changes in global neuronal activity. To determine the NR2B-containing NMDAR surface distribution, the relative content of synaptic, perisynaptic (300-nm annulus around the synapse), and extrasynaptic detected molecules was quantified. In control conditions, 21 ± 4% of molecules were synaptic, 15 ± 3% perisynaptic, and 64 ± 6% extrasynaptic ($n = 23$ dendritic fields). After a chronic incubation of neurons from D9 to D15 with an NMDAR antagonist (50 μM AP-5), a $GABA_A$ receptor channel blocker (100 μM picrotoxin), or a sodium channel blocker [1 μM tetrodotoxin (TTX)], NR2B-containing NMDAR surface distribution did not significantly change ($P > 0.05$ in all conditions) (Fig. 4*b Middle*). Moreover, the surface diffusion of NR2B-containing NMDARs remains unaffected by these treatments (Fig. 4*b*). All together, these results indicate that the surface distribution and diffusion of NR2B-containing NMDARs are developmentally regulated in an activity-independent manner.

Differential Stability of NR2A- and NR2B-Containing NMDARs Within Synapses Overdevelopment. The decreased content of surface synaptic NR2B-containing NMDAR overdevelopment could come from several processes, i.e., a restriction of NR2B-containing NMDAR to enter laterally the synapse, a lack of stabilization of the receptor within the postsynaptic membrane, or a change in the cycling rate of NR2B-containing NMDAR between intracellular and membrane pools. To test these possibilities, we first measured the exchange rate of the NR2B-containing NMDARs that alternate between the extrasynaptic and synaptic membranes (Fig. 5*a*). The percentage of exchanging NR2B-containing NMDARs at D15 (29%) was slightly higher than at D8 (22%) and than for NR2A-containing NMDARs at D15 (22%). The exchange rate, defined as the number of compartment changes over a time period (60 s), and the synaptic dwell time, defined as the mean time spent by exchanging receptor within the synaptic area, were calculated. The exchange rate of NR2B-containing NMDARs was not significantly different at D8 and D15, remaining at ≈0.6 Hz (≈36 compartment changes per min) (Fig. 5*b*), ruling out a potential restriction of NR2B-containing receptors to laterally enter mature synapses. We then measured the residency time of exchanging NR2B-containing NMDARs within synapses to estimate receptor stabilization within the postsynaptic membrane. Interestingly, the residency time was significantly decreased by a factor of three from D8 to D15 (Fig. 5*c*), indicating a higher surface stabilization of NR2B-containing NMDAR in early synapses when compared with more mature ones. It can be noted that at D15 the residency time of NR2A-containing NMDAR was significantly higher than that of NR2B-containing NMDAR, indicating a better stabilization of NR2A-containing NMDAR within mature synapse. We thus propose that the relative decreased content of NR2B-containing NMDAR within mature synapse is due to instability of the surface receptor within the postsynaptic membrane. Finally, the observed decreased content of surface synaptic NR2B-containing NMDAR overdevelopment that would come from an increased internalization of the receptor is unlikely because NR2B-containing NMDAR internalization remains constant overdevelopment (from D5 to D12) (17). Along this line, we measured the internalization rate of all NMDARs by using an anti-NR1 antibody directed against an extracellular epitope (19) (*Supporting Methods*) and found that the internalization of NMDARs during development is significantly decreased (D8: 32 ± 3% of internalized NR1-containing NMDARs, $n = 5$; D15: 10.5 ± 5%, $n = 5$; $P < 0.05$). Thus, the decreased contribution of synaptic NR2B-containing NMDARs is not due to an increased internalization of NMDAR overdevelopment.

Discussion

In the present study, we show that part of the surface mobility of NMDARs depends on the NR2A-2B subunit subtype, NR2A-containing NMDARs being more stable than NR2B-containing ones. The synaptic composition of NMDARs changed over maturation with an increase in the NR2A/NR2B subunit ratio. Interestingly, the developmental switch in the synaptic NR2A- and NR2B-containing NMDAR surface distribution correlates with developmental changes in the time spent by subunits within synapses without any change in the lateral exchange of the receptors (Fig. 5*f*). These data shed light on how surface NR2A- and NR2B-containing NMDARs can be differentially trafficked and they propose a developmental model in which the regulation of synaptic NMDAR subtypes depends on the synaptic surface stabilization of the receptors.

Our current knowledge of the differential distribution of NR2A and NR2B-containing NMDARs at the neuronal surface has come from either electrophysiological approaches or detection of genet-

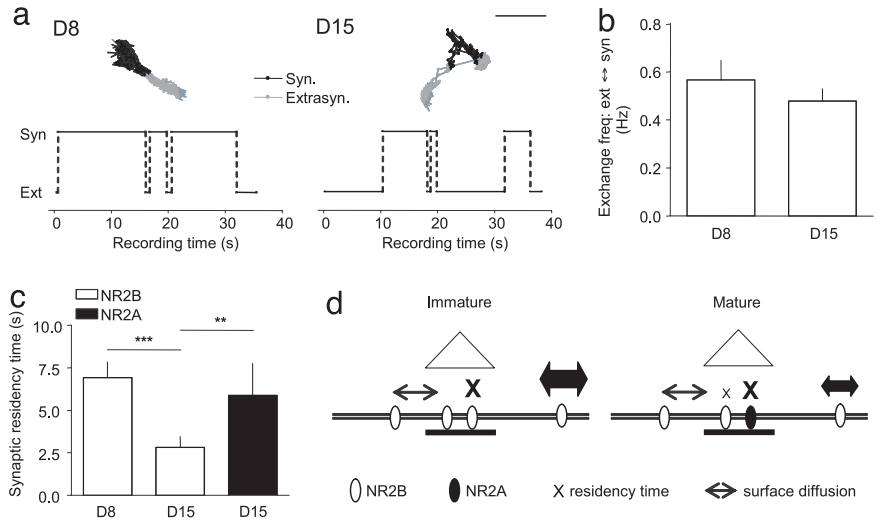

Fig. 5. Exchange rate and synaptic dwell-time of NR2B-containing NMDARs overdevelopment. (*a*) Surface trajectory of two NR2B-containing NMDARs at D8 and D15. The NMDARs exchanged between the synaptic (black line) and extrasynaptic (gray line) membrane compartments. (Scale bar: 300 nm.) Recordings of the NR2B-containing NMDAR compartment localization over time at D8 and D15. In these two examples, the NR2B-containing NMDARs exchange approximately three to four times between the synaptic (Syn) and extrasynaptic (Ext) compartments during the 35- to 40-s recording. (*b*) Exchange rate (mean ± SEM, Hertz) between the extrasynaptic and synaptic compartments was calculated for NR2B-containing NMDARs at D8 ($n = 17$) and D15 ($n = 18$). (*c*) Synaptic residency time of exchanging NR2A- ($n = 18$) and NR2B-containing NMDARs was measured and compared overdevelopment (mean ± SEM, seconds). Note the significant decrease for NR2B-containing NMDARs overdevelopment. At mature stages, the synaptic residency time of NR2A-containing NMDARs was similar as the one of NR2B-containing NMDARs at immature stages. (*d*) Schematic representation of the regulation of NR2A- and NR2B-containing NMDAR surface diffusion over neuronal maturation. The synapse is represented by the presynaptic element (open triangle) and the postsynaptic density (filled bar).

ically engineered NR2 subunits (2). The antibodies directed against NR2A or NR2B subunit extracellular epitopes allowed the direct investigation of the surface mobility of native, and not genetically engineered, NR2A and NR2B subunits. The observed surface distributions for both native subunits are consistent with the current model in which neurons express NR2B-containing NMDAR early in development with both extrasynaptic and synaptic localizations, whereas NR2A-containing NMDAR expression appears later and are restricted to synapse, although present in the extrasynaptic membrane (present study; refs. 5 and 9). The data show a colocalization of both NR2 subunits in mature synapses, indicating various possible combinations for NMDAR composition, including the well described triheteromeric one (1, 5, 9, 10, 12–14). The surface diffusion of NMDARs has been described by single-molecule tracking (19) and by electrophysiological means (18). In the present study, the use of individual nanometer-sized fluorescent objects, the QDs, uniquely allow the tracking of individual or small assemblies of surface NMDARs for long recording periods in various membrane compartments, including confined spaces (e.g., synaptic cleft) (19, 23, 28). It further provides a way to measure the time spent by NMDAR in a specific membrane compartment, i.e., extrasynaptic and synaptic membranes, and to quantify the lateral exchange rate between membrane compartments. It can be noted that surface extrasynaptic NR2A-containing NMDARs were not observed by immunocytochemical means, whereas they were detected and tracked by single-molecule/particle approaches, indicating a lower detection threshold for the latter (29) and the presence of NR2A-containing NMDARs outside synapse (9). Although NR2B-containing NMDARs outnumbered NR2A-containing NMDARs in the extrasynaptic membrane, we found a similar proportion of exchanging NR2B- and NR2A-containing NMDARs between the extrasynaptic membrane and synapse, in which they were only temporary stabilized. Such a result suggests that the surface distribution of NR2A- and NR2B-containing NMDARs also likely result from differences in cycling processes (outside synapse) between intracellular and membranes receptor pools (17, 30, 31).

Differences in surface diffusion of NR2A- and NR2B-containing NMDARs are likely the result of multiple cellular processes, including binding affinity to scaffold proteins, phosphorylation state of the NR subunits, and/or extracellular factors. Two membrane-associated guanylate kinases (MAGUKs), synapse associated protein 102 (SAP-102) and postsynaptic density 95 (PSD-95), which both contribute to form a scaffold for ionotropic glutamate receptors at the postsynaptic density, indeed have been proposed to play a role in the NMDAR subunit switch during development (4). Schematically, a preference of certain MAGUKs for different NMDAR subtypes suggest that different NMDAR scaffolding proteins could affect the trafficking and synaptic localization of NR2A- and NR2B-containing NMDARs during synaptic development (11, 32, 33). In this model, NR2A-containing NMDARs are synaptically incorporated, PSD95 is inserted into the center of the postsynaptic density and displaces the NR2B subunit–SAP102 complexes, which were initially located at the postsynaptic density, to the perisynaptic and extrasynaptic membranes (32, 34, 35). Our current data on the surface mobility of NR2A/B subunits support this hypothesis and further indicate that the lateral shift of the subunits observed by electrophysiological means likely results from differences in lateral mobility and stabilization of the subunits. Indeed, surface NR2A-containing NMDARs are more stable than NR2B-containing ones within mature synapses, possibly due to a high proportion of PSD-95 over SAP-102 in the postsynaptic density. Interestingly, the domains on the C-terminal tail are critical to retain NR2A- (36) and NR2B-containing NMDARs (30) within synapses and the binding of NMDARs to PDZ proteins is a regulated process, depending on kinase activation (37), suggesting that NR2A/B surface mobility is indeed dynamically regulated by intracellular interactions. To The synaptic retention of NMDARs also depends on extracellular factors such as the EphB receptor, which interacts with NMDARs through N-terminal extracellular domains (38), cell-adhesion molecules (e.g., integrins) (39), and proteins of the extracellular matrix (e.g., reelin) (40). Interestingly, the type of presynaptic neuron is a critical determinant of the subunit composition of NMDARs expressed at synapses (41), suggesting that appropriate expression of molecules in both pre- and postsynaptic compartments is necessary for NMDAR maturation.

In conclusion, the surface mobility of NMDARs depends, in part, on the NR2A versus 2B subunit composition. The presence of triheteromeric structure (NR2A and NR2B subunits) or other NR subunits such as NR3A early in development (42) is also likely to play a role in determining surface mobility of NMDARs. Our results unravel a way to differentially traffic NR2A- and NR2B-containing NMDARs at the neuronal surface and indicate that the maturation of excitatory glutamate synapses is accompanied by changes in the stability of specific NMDAR subtypes.

Methods

Cell Culture, Synaptic Live Staining, and Protein Expression in Neurons. Preparation of the cultured neurons for single molecule/particule staining has been done as described in refs. 19 and 24.

Schematically, hippocampal neurons from 18-day-old rat embryos were cultured on glass coverslips by following the Banker technique. To label synapses, neurons were incubated for 1–2 min at 20°C with 1 nM Mitotracker (Deep Red-Fluorescent Mitotracker; Molecular Probes, Leiden, The Netherlands). For protein expression, days *in vitro* 10–15 hippocampal-cultured neurons were transducted 24–36 h before experiment by using Lipofectamine 2000 reagent (Invitrogen, Carlsbad, CA). SEP-NR2A and SEP-NR2B cDNAs were constructed by fusing the superecliptic pHluorin (enhanced mutant of pH-sensitive GFP) to the N terminus of rat NR2A and NR2B subunits, respectively. For transfection, culture coverslips were incubated with ≈1 μg cDNA for 40 min at 37°C. The superecliptic pHluorin allow the specific visualization of surface SEP-NR subunits (43, 44), which ensure that the overexpressed proteins were well targeted to the plasma membrane.

Immunocytochemistry. Surface NR2A or NR2B subunits were stained specifically by using the newly developed rabbit polyclonal antibodies. Briefly, neurons were fixed with 4% paraformaldehyde and incubated with 6 μg of affinity-purified antibodies directed against NR2A or NR2B subunits for 30 min. The primary antibodies were revealed by using anti-rabbit Alexa 568 antibodies (8 μg for 2–3 h). To label synaptic sites, neurons then were permeabilized by using 0.3% Triton X-100, incubated with a rabbit polyclonal anti-synaptotagmin antibody (6 μg for 1 h), followed by secondary incubation with a anti-rabbit Alexa 488 antibodies (5 μg for 30 min). For the surface fluorescence quantification, the average total intensity and the pixel area were measured within only dendritic field (soma excluded from analysis). For the colocalization measurement, the pixel area of synaptotagmin and NR2 subunit staining were compared, and the percentage of overlap between the two was calculated. The fluorescence analysis was realized by using Metamorph software (Universal Imaging, Downingtown, PA).

Single-Molecule and -Particle (QD) Tracking. Cyanine 3 was coupled to the affinity-purified rabbit polyclonal anti-NR2A or anti-NR2B antibodies that are both directed against extracellular epitopes of NR2 subunits. All neurons, which are mainly excitatory ones, were incubated for 10 min at 37°C with the respective cyanine–antibody complexes. As described in ref. 19, all recording sessions were acquired within 30 min after primary antibody incubation to minimize receptor endocytosis. Single-molecule detection was realized as described in refs. 19 and 24. Briefly, a custom wide-field single-molecule fluorescence inverted microscope equipped with a ×100 oil-immersion objective was used. The samples were illuminated for 30 msec at a wavelength of $\lambda = 532$ nm by a frequency doubled YAG laser (Coherent, Les Ulis, France) at a rate of 15 Hz. Appropriate filter combination (DCLP550, HQ600/75; Chroma Technology, Brattleboro, VT) allowed the detection of individual fluorophore by a CCD camera system (Micromax; Princeton Instruments, Trenton, NJ). Using the same excitation path, Red Deep Mitotracker (Molecular Probes) was excited with the $\lambda = 633$ nm line of a He-Ne laser (JDS Uniphase, Manteca, CA) at an illuminating intensity of 7 ± 1 kW/cm^2. We imaged and resolved discrete fluorescence spots (45). Fluorescence spots exhibit one-step photobleaching and not gradual decay as for ensemble photobleaching. We calculated the instantaneous diffusion coefficient, D, for each trajectory, from linear fits of the first four points of the mean-square-displacement versus time function by using $\mathrm{MSD}(t) = \langle r^2 \rangle (t) = 4Dt$. The 2D trajectories of single molecules in the plane of focus were constructed by correlation analysis between consecutive images by using a Vogel algorithm. For QD tracking, QD 655 Goat F(ab′)2 anti-Rabbit IgG (0.1 μM; Ozyme, Paris, France) first were incubated for 30 min with the polyclonal antibodies against NR2A (1 μg) and NR2B subunits (1 μg). Nonspecific binding was blocked by additional casein (Vector Laboratories, Paris, France) to the QD 15 min before use. Neurons were incubated for 10 min at 37°C in culture medium with precoated QD (final dilution 0.1 nM). QDs were detected by using a xenon lamp (excitation filter HQ500/20X (Chroma Technology; Mitotrack) 560RDF55 (Omega, QD) and appropriate emission filters [respectively, HQ560/80M (Chroma Technology), and 655WB20; Omega Filters]. Images were obtained with an integration time of 50 msec respectively with up to 1200 consecutive frames. Signals were detected by using a CCD camera (Cascade; Princeton Instruments). QD-labeled NR2 subunits were followed on randomly selected dendritic regions for up to 30 min. The trajectory reconstruction was carried out as for single-molecule tracking (see above).

We thank Martha Constantine-Paton and Cansu Tunca (Massachusetts Institute of Technology, Boston, MA) for the gift of wild-type and NR2A (−/−) mouse brains, Jacques Neyton (École Normale Supérieure, Paris, France) for cDNA constructs, Carlos Dotti (University of Leuven, Leuven, Belgium) for synaptotagmin antibodies, Kieran Brickley for animal immunizations, Pascale Chavis for critical reading of the manuscript, and Mike D. Ehlers for helpful discussions. This work was supported by grants from the Centre National de la Recherche Scientifique, The Conseil Régional d'Aquitaine, The Ministère de la Recherche, European Community Grant CT-2005-005320 (Glutamate Receptor Interacting Proteins as Novel Neuroprotective Targets), and the Biotechnology and Biological Sciences Research Council (U.K.).

1. Sheng M, Cummings J, Roldan LA, Jan YN, Jan LY (1994) *Nature* 368:144–147.
2. Wenthold RJ, Prybylowski K, Standley S, Sans N, Petralia RS (2003) *Annu Rev Pharmacol Toxicol* 43:335–358.
3. Nowak L, Bregestovski P, Ascher P, Herbet A, Prochiantz A (1984) *Nature* 307:462–465.
4. van Zundert B, Yoshii A, Constantine-Paton M (2004) *Trends Neurosci* 27:428–437.
5. Tovar KR, Westbrook GL (1999) *J Neurosci* 19:4180–4188.
6. Monyer H, Burnashev N, Laurie DJ, Sakmann B, Seeburg PH (1994) *Neuron* 12:529–540.
7. Carmignoto G, Vicini S (1992) *Science* 258:1007–1011.
8. Liu XB, Murray KD, Jones EG (2004) *J Neurosci* 24:8885–8895.
9. Thomas CG, Miller AJ, Westbrook GL (2006) *J Neurophysiol* 95:1727–1734.
10. Luo J, Wang Y, Yasuda RP, Dunah AW, Wolfe BB (1997) *Mol Pharmacol* 51:79–86.
11. Shi J, Aamodt SM, Constantine-Paton M (1997) *J Neurosci* 17:6264–6276.
12. Kew JN, Richards JG, Mutel V, Kemp JA (1998) *J Neurosci* 18:1935–1943.
13. Stocca G, Vicini S (1998) *J Physiol* 507:13–24.
14. Li JH, Wang YH, Wolfe BB, Krueger KE, Corsi L, Stocca G, Vicini S (1998) *Eur J Neurosci* 10:1704–1715.
15. Barria A, Malinow R (2002) *Neuron* 35:345–353.
16. Roche KW, Standley S, McCallum J, Dune Ly C, Ehlers MD, Wenthold RJ (2001) *Nat Neurosci* 4:794–802.
17. Lavezzari G, McCallum J, Dewey CM, Roche KW (2004) *J Neurosci* 24:6383–6391.
18. Tovar KR, Westbrook GL (2002) *Neuron* 34:255–264.
19. Groc L, Heine M, Cognet L, Brickley K, Stephenson FA, Lounis B, Choquet D (2004) *Nat Neurosci* 7:695–696.
20. Chazot PL, Cik M, Stephenson FA (1995) *Mol Membr Biol* 12:331–337.
21. Papadakis M, Hawkins LM, Stephenson FA (2004) *J Biol Chem* 279:14703–14712.
22. Thompson CL, Drewery DL, Atkins HD, Stephenson FA, Chazot PL (2000) *Neurosci Lett* 283:85–88.
23. Dahan M, Levi S, Luccardini C, Rostaing P, Riveau B, Triller A (2003) *Science* 302:442–445.
24. Tardin C, Cognet L, Bats C, Lounis B, Choquet D (2003) *EMBO J* 22:4656–4665.
25. Li B, Otsu Y, Murphy TH, Raymond LA (2003) *J Neurosci* 23:11244–11254.
26. Lindlbauer R, Mohrmann R, Hatt H, Gottmann K (1998) *J Physiol* 508:495–502.
27. Fu Z, Logan SM, Vicini S (2005) *J Physiol* 563:867–881.
28. Howarth M, Takao K, Hayashi Y, Ting AY (2005) *Proc Natl Acad Sci USA* 102:7583–7588.
29. Triller A, Choquet D (2005) *Trends Neurosci* 28:133–139.
30. Prybylowski K, Chang K, Sans N, Kan L, Vicini S, Wenthold RJ (2005) *Neuron* 47:845–857.
31. Li B, Chen N, Luo T, Otsu Y, Murphy TH, Raymond LA (2002) *Nat Neurosci* 5:833–834.
32. Yoshii A, Sheng MH, Constantine-Paton M (2003) *Proc Natl Acad Sci USA* 100:1334–1339.
33. Sans N, Petralia RS, Wang YX, Blahos J, II, Hell JW, Wenthold RJ (2000) *J Neurosci* 20:1260–1271.
34. Townsend M, Yoshii A, Mishina M, Constantine-Paton M (2003) *Proc Natl Acad Sci USA* 100:1340–1345.
35. Shi J, Townsend M, Constantine-Paton M (2000) *Neuron* 28:103–114.
36. Steigerwald F, Schulz TW, Schenker LT, Kennedy MB, Seeburg PH, Kohr G (2000) *J Neurosci* 20:4573–4581.
37. Chung HJ, Huang YH, Lau LF, Huganir RL (2004) *J Neurosci* 24:10248–10259.
38. Dalva MB, Takasu MA, Lin MZ, Shamah SM, Hu L, Gale NW, Greenberg ME (2000) *Cell* 103:945–956.
39. Chavis P, Westbrook G (2001) *Nature* 411:317–321.
40. Sinagra M, Verrier D, Frankova D, Korwek KM, Blahos J, Weeber EJ, Manzoni OJ, Chavis P (2005) *J Neurosci* 25:6127–6136.
41. Gottmann K, Mehrle A, Gisselmann G, Hatt H (1997) *J Neurosci* 17:2766–2774.
42. Perez-Otano I, Lujan R, Tavalin SJ, Plomann M, Modregger J, Liu XB, Jones EG, Heinemann SF, Lo DC, Ehlers MD (2006) *Nat Neurosci* 9:611–621.
43. Kopec CD, Li B, Wei W, Boehm J, Malinow R (2006) *J Neurosci* 26:2000–2009.
44. Ashby MC, Ibaraki K, Henley JM (2004) *Trends Neurosci* 27:257–261.
45. Schmidt T, Schutz GJ, Baumgartner W, Gruber HJ, Schindler H (1995) *J Phys Chem* 99:17662–17668.